Engineering Science and Technology, an International Journal 24 (2021) 1262–1271

HOSTED BY

Contents lists available at ScienceDirect

Engineering Science and Technology, an International Journal

journal homepage: www.elsevier.com/locate/jestch

Full Length Article

Horizontal end crack control and load-bearing capacity performance of hollow-type pretensioned girders through experimentally calibrated finite element models

Bashir Ahmad Aasim [a,b], Abdul Khaliq Karimi [a,b], Jun Tomiyama [a], Yuya Suda [a]

[a] Department of Civil Engineering and Architecture, University of the Ryukyus, Senbaru, 1, Nishihara, Nakagami District, Okinawa 903-0213, Japan
[b] Civil Engineering Department, Kandahar University, New Eidga, Loya Weyala, Kandahar, Afghanistan

ARTICLE INFO

Article history:
Received 3 July 2020
Revised 23 January 2021
Accepted 8 February 2021
Available online 27 February 2021

Keywords:
Prestressed concrete
Hollow-type PC girder
Horizontal end cracks
Load-bearing capacity
Midas FEA

ABSTRACT

Prestressed concrete girders are prone to the formation of horizontal end cracks during prestress transfer. These cracks propagate and progress extensively in deeper hollow-type pretensioned girders with larger prestressing forces. This study examines the strand-debonding method to eliminate horizontal cracks at the ends of hollow–type pretensioned girders by directly reducing the vertical tensile stresses resulting from the prestress release acting on the strands. Finite element analysis is adopted to model the girder and identify the cracking zone in the cross-section. Furthermore, the load-bearing capacity of the girder is investigated through a four-point bending test using construction stage analysis in a numerical simulation. The numerical results are validated through fabrication of an actual girder with geometrical and mechanical specifications identical to those in the numerical model. The experimental findings match the numerical results; the horizontal end cracks diminish with the application of the proposed method. Furthermore, the study confirms the normal behavior of the girder against vertical loading; the girder can resist the load, similar to a girder with an ordinary cross-section.

1. Introduction

The Prestressing is considered the most significant new direction in structural engineering, especially in bridge design, for its long service life and limited maintenance cost [1–5]. However, prestressing has existed for some time. David P. Billington presented the history of prestressed concrete in four stages, reporting that the first prestressed structures were designed and erected in the United States in 1829–1830, and the first iron structure was designed in Europe in 1836 [6,7]. The first prestressed concrete bridge in Japan was constructed in 1953 and is still in use without any major deficiencies. Despite the rapid development of prestressed concrete and its importance in structural engineering, prestressed concrete members still pose some challenges in their functioning behavior. Prestressed concrete construction can be performed by prestressing the strands, and is classified as pretensioning or post-tensioning [8].

Pretensioned concrete girders are favored over other superstructure members because they efficiently span longer distances as a result of their higher load–carrying capacity. Several factors influence pretensioned girders after the cast concrete develops the required initial strength. Tendon–concrete bond performance is a dominant parameter that causes horizontal cracks when the strands release.

Pretensioned girder end zones, where the prestress transfer occurs, often exhibit characteristic horizontal cracking during or immediately after the application of prestress to the concrete. The prestress transfer from the wire to the concrete at the ends of the pretensioned girders creates a region of stress concentration [9–11], resulting in the formation of cracks during detensioning. The cracks appear to be more severe in recently developed heavily prestressed hollow girders, as shown in Fig. 1.

Cracks with smaller dimensions are acceptable and can be sealed; girders with larger cracks present durability concerns [4] as they provide pathways for the ingress of chlorides that compromise the bond mechanisms between strands and concrete at the ends [2]. The prestress force is gradually transferred through bonding between the steel and concrete over a distance known as the transfer length. The transfer length is defined as the bond length required to fully transfer the effective prestress from the strands to the concrete [5,8]. Through bond effects, compressive stresses radiate from the strands into the concrete. A zone of compressive stress develops radially toward the strands. The dispersion of

E-mail address: bashir.aasim@kdru.edu.af (B.A. Aasim)

https://doi.org/10.1016/j.jestch.2021.02.007
2215-0986/

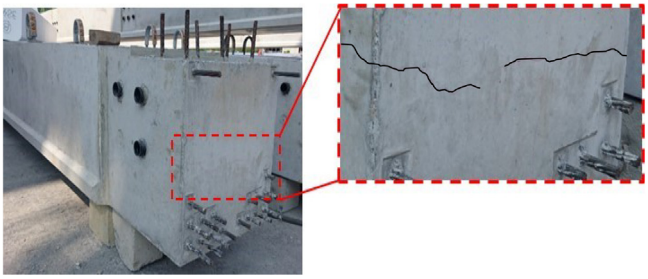

Fig. 1. Location and pattern of horizontal end cracks in hollow–type girder.

compressive stresses causes tensile stresses to develop normally in the direction of the prestressing strands. If the magnitude of these vertical tensile stresses (principal stresses) is greater than the tensile strength of the concrete, horizontal cracks develop at the ends of the pretensioned girders. Compressive stresses propagate into the member in a curved pattern until a linear stress distribution results [9–11]. The end zone stress distribution in a pretensioned concrete girder is a function of the location and magnitude of the prestressing strands, the degree of bond between the strands and the surrounding concrete, the amount of strand draping in the end zone, the section geometry, and the concrete material properties [12].

The stress conditions in pretensioned beams are usually less severe than in post–tensioned beams because the prestress force is introduced gradually; however, the tensile stresses that develop are often large enough to cause cracks in the member. Horizontal end cracks in pretensioned bridge girders are a concern for girder manufacturers and designers [4]. The cracks are most visible while lifting the girders from the prestressing bed, shortly after the prestress release. The bridge supports at the end of the girder are susceptible to corrosion through the deck expansion joints above the girders at the ends of the bridge. Girder durability problems may include corrosion of steel rebar or strands and lead to adverse effects on the structural capacity [13–16]. Girders manufactured with cracks may increase maintenance costs over the bridge service life and may be structurally hazardous if corrosion agents flow along the prestressing strands [17,18]. End zone cracks have been observed in girders of different shapes including box girders, I-shaped girders, hollow slabs, and tee beams [19]. Several studies have been conducted to control horizontal cracking at the girder ends. However, there is little research on hollow–type girders, which are vulnerable to the development of horizontal end cracks from prestressing forces [20].

This study applies the strand–debonding method to eliminate horizontal cracking at the ends of a pretensioned hollow–type BS12 girder through finite element analysis (FEA) software and experiments. Several approaches adopted in previous studies can reduce principal stresses, including strand configuration in the cross–section, end zone reinforcement alongside the strand–debonding, strand–cutting order, and draped strands [12,21]. These studies were conducted on ordinary, non–hollow sections. This study demonstrates that only the strand–debonding method can effectively eliminate horizontal end cracks in a BS12 girder and similar girders. The approach involves debonding a few strands at the ends of the girder to transfer the prestressing load of the debonded portion further into the girder length. The debonding process is performed by placing a plastic sheath around the strand to remove the bond between the strands and the concrete. Debonding certain strands reduces the magnitude of the principal stresses at the ends of the girder, which is the main cause of horizontal cracking. It is extremely important to consider the number of debonded strands, their debonded lengths, and their release patterns. Although the debonding method has been found to be generally safe, these factors can have a significant impact if they are not carefully considered. The cracks occur during prestress application, which can affect the long–term durability of the girder, especially in a saline environment, and result in serious damage. To avoid this problem, methods to prevent cracking in various types of girders must be developed. The BS12 girder was selected for this study for its research feasibility, ease of manufacturing, and limited references in the literature.

After selecting the girder type, numerical simulations were performed using Midas FEA software to model the girder and evaluate the horizontal end cracks and the vertical principal stress distributions at the ends of the girder. The main cause of horizontal cracks in the girder end zones is principal stress exceeding the tensile strength during the prestress release stage [23]. Debonding selected strands can reduce the principal stresses, eliminating horizontal end cracks. Prior to physical specimen preparation, two models of the girder were created in Midas FEA with identical parameters. All strands were fully bonded in one model; four alternating strands were debonded in the other model to evaluate their reaction.

There was concern regarding the load–bearing capacity of this type of girder. With a longitudinal hole at the cross–section, there was a possibility that the girder might not perform as well against vertical loading as one with an ordinary cross–section. To check the load–bearing capacity of the BS12 girder, a numerical model of the girder was analyzed through a construction stage analysis using Midas FEA; a four–point bending test was conducted on the actual girder to verify the FEA results.

Based on the numerical and experimental results, the proposed debonding method was found to be convenient and suitable for preventing horizontal cracking at the ends of BS12 and similar girders. Moreover, the results showed that girders with hollow–type cross–sections can resist vertical loads, similar to girders with ordinary cross–sections.

2. Description of girder

The specimen in this study is a pretensioned prestressed hollow–type BS12 girder with a hole in the middle of the cross–section along its entire length, resulting in a considerable decrease in the amount of concrete, as shown in Fig. 2a. The girder is simply

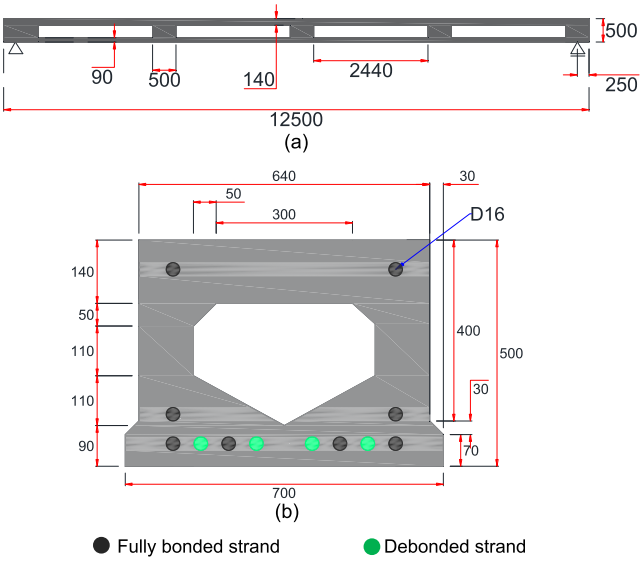

Fig. 2. (a) Longitudinal section with five diaphragms; (b) Cross–section showing strands position and hollow part of the girder (mm).

supported across an effective span of 12 m with a cross–section of 700 mm × 500 mm, as shown in Fig. 2b. It is reinforced with 12 longitudinal PC strands with a nominal diameter of 15.2 mm; ten strands are distributed in the lower flange in the tension zone and two are placed in the compression zone of the section. SD295–type steel bars with a 200 GPa elastic modulus and a 10 mm diameter (D10) are used for transverse reinforcement and placed in 100 mm, 150 mm, and 200 mm spacing along the girder, as shown in Fig. 3. Fig. 4 shows the constitutive model of the selected steel bars, which is an elastic–perfectly plastic model that requires only an initial yield condition. SWPR7BL PC strands meeting the JIS G 3536 standard with an elastic modulus of 200,000 N/mm^2 and a 138.7 mm^2 cross–sectional area are selected [24]. The allowable stress for the PC strands is 1440 N/mm^2; some relaxation occurs after prestressing, reducing the stress to 1295 N/mm^2. After detensioning, the axial force is transferred to the concrete and the pretensioning stress decreases to 1110 N/mm^2 in the strands [22]. Table 1 lists the sectional parameters and locations of the strands in the girder.

3. Pretensioning

In pretensioned girders, cracks appear immediately after the prestress is released in the construction process without the application of an external load. Thus, the main loading considered for nonlinear static analysis in numerical modeling is the prestressing force. According to the Japan Road Association (JRA) specifications for concrete bridges (2012), the transfer length should be approximately 65 times the diameter of the strands [26]. The strands in this study were 15.2 mm in diameter, and the transfer length in the models was calculated to be 988 mm. Stresses in the concrete were zero at the ends of the girder where the strand slip occurred. At the end of the transfer length, the concrete carried the full effective prestress from the strands, as shown in Fig. 5. Prestressing force was directly applied to the strands, assuming them to be the truss elements in this model; a 187.2 kN prestressing force was introduced to each strand after confirmation of 70% of concrete compressive strength through testing of cylindrical concrete samples, as shown in Figs. 6 and 7.

The stresses transferred from the strands produced longitudinal axial stresses in the concrete at the strand release. These are known as effective stresses, and were calculated using Eq. (1) based on JIS A 5373 2010.

$$\sigma_{ct} = \sigma_{pt} \times \sum A_p \times \left(\frac{1}{A'} + \frac{Y_e}{Z}\right) \quad (1)$$

where σpt denotes the prestress acting on the strands immediately after strand tensioning, $\sum A_p$ is the cross-sectional area of all PC strands, A' represents the cross-sectional concrete area, Y_e is the distance from the bottommost fiber to the neutral axis of the transformed section, and Z is the section modulus of the bottommost fiber. The effective stress design value at the bottommost fiber of the girder is 16.7 N/mm^2, as calculated from Eq. (1).

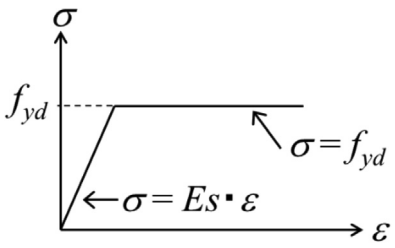

Fig. 4. Constitutive law for reinforcement [25].

4. Numerical study

4.1. Finite element analysis

Finite element analysis is the primary tool used to predict cracking behavior at the ends of pretensioned hollow–type girders. One of the major advantages of finite element analysis is the ability to obtain information for the entire domain of the model, in contrast to experiments in which information is obtained only from measurement locations and data sampling at selected times. FEA can provide reactions of the structure under arbitrary loading in the form of strains and stresses in any direction. Understanding the evolution and distribution of principal stresses is of particular importance in this research. The principal stresses determine where and to what extent cracking may occur. Plastic principal tensile strains and strain paths are another way to interpret the cracks and explain the behavior near the girder ends. The concrete material properties listed in Table 2 were obtained from the compressive strength according to Eqs. (2)–(4) [25]:

$$f_t = 0.23 \times f_c^{\frac{2}{3}} \quad (2)$$

$$G_t = 10 \times d_{max}^{\frac{1}{3}} \times f_c^{\frac{1}{3}} \quad (3)$$

$$G_c = 8.8 \times f_c^{\frac{1}{2}} \quad (4)$$

where f_t is the tensile strength, G_t is the tensile fracture energy, G_c is the compressive fracture energy, d_{max} mm is the maximum size of coarse aggregate, and f_c is the concrete compressive strength

4.2. Nonlinear analysis

EA software was used to simulate the girder end behavior. The models were prepared to investigate the factors influencing the principal stresses in prestressing that produce horizontal cracking at the ends of the BS12 girder. These factors include the number, position, and length of the debonded strands. To examine these parameters, two girder models with identical characteristics and material properties were considered.

Two types of concrete material properties (for nonlinear and construction stage analysis) are listed in Table 2. In Case #1, all strands of the girder were fully bonded. In Case #2, four alternating

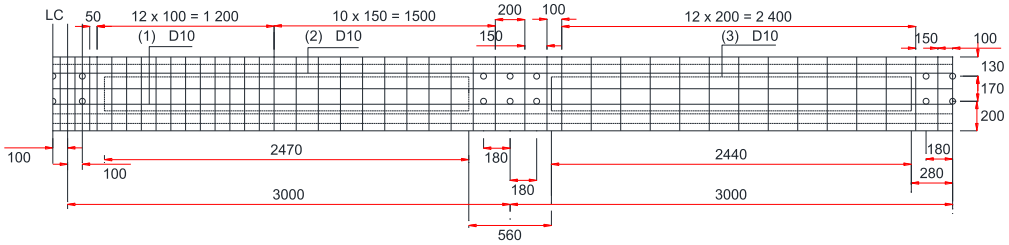

Fig. 3. Stirrup placement plan and spacing in the girder.

Table 1
Sectional parameters for BS12 girder [22].

	Concrete Cross–section Area A(mm^2)	Distance from centroid			Geometrical moment of inertia I (mm^4)	Section modulus		
		Upper surface y'(mm)	Bottom surface y (mm)	Centroid of PC strand Y(mm)		Upper SurfaceZ'_c (mm^3)	Bottom surface Z_p(mm^3)	Centroid of PC strands Z_p(mm^3)
Concrete section	241,600	253.5	−246.5	−119.0	6.53×10^9	2.58×10^7	-2.65×10^7	-5.49×10^7
Transformed section	250,023	257.5	−242.5	−115.0	6.82×10^9	2.65×10^7	-2.82×10^7	-5.94×10^7

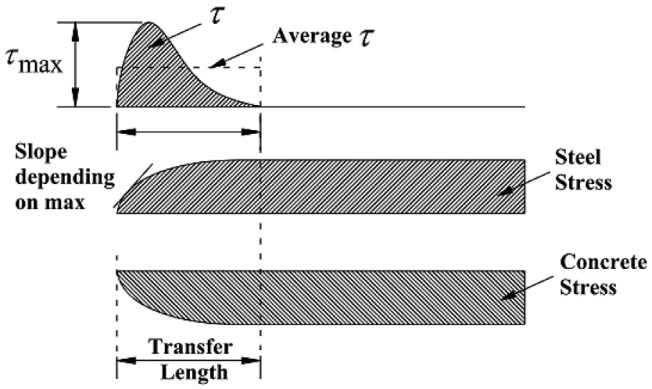

Fig. 5. Bond stress distribution at the strand end [27].

Fig. 6. Concrete samples for compressive testing.

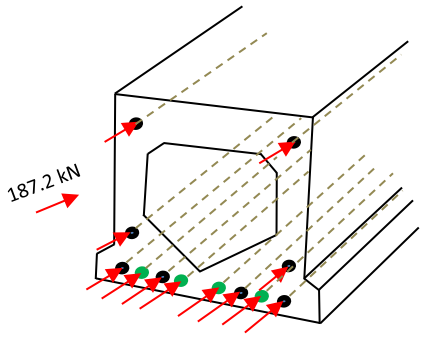

Fig. 7. Applied forces on PC strands.

strands in the lower flange were debonded, as shown in Fig. 8. Osman and French reported that the maximum number of debonded strands in a cross-section should be 40% of the strands or four strands [28]. As the girder section was symmetric, with eight strands in the bottom row, four alternating strands were selected for debonding to reduce the principal stresses equally in the cross–section of the girder.

Nonlinear FEA of concrete cracking simulations can be computationally expensive in terms of time and storage space [3]. Thus, for efficient computation, only one–quarter of the girder was simulated in FEA considering the double symmetry in the applied loading, geometry, and boundary conditions. Fig. 9 shows sectional views, reinforcement model, and the degrees of freedom at the boundaries. Considering the symmetry condition, translation in the Z direction was restricted at the end of the model; translation at the midpoint of the symmetry edges was restricted to the X–Y plane, but the model was free to rotate in all three directions.

In the modeling, concrete, loading, and supporting plates were modeled using three–dimensional hexahedral elements. Truss elements represent the PC strands; compressive forces were applied to the truss elements as prestressing forces; the steel bars used as stirrups were modeled using embedded reinforcement bar elements.

4.3. Construction stage analysis

A four–point bending test was conducted using construction stage analysis in the Midas FEA software to evaluate the load–bearing capacity of the girder. The girder was assumed to be a beam–like structure with simply supported boundary conditions, as shown in Fig. 10. The concrete material properties adopted for nonlinear analysis correspond to the concrete not attaining its full strength. For the construction stage analysis, the bending test parameters were selected such that the concrete attained its full strength. The constitutive laws for the materials in the analysis are shown in Fig. 11. Bond stress and slipping threshold were assumed to be 5.0 N/mm^2 and 0.2 mm, respectively, and these values were selected based on a parametric analysis (pre–analysis) [19].

5. Numerical results

5.1. Nonlinear analysis results

To examine the stress state associated with horizontal cracking at the ends of the BS12 girder, the stress contour, principal stresses along the vertical edge of the end section, and crack locations are shown in Figs. 12 and 13. In Case #1, with all strands fully bonded, the principal stresses in the end zones of the girder were greater than the tensile strength of the concrete, and horizontal cracks were likely to occur near the middle of the outer edge, as shown in Fig. 14. However, debonding four alternating strands in the first row of the lower flange reduced the principal stress below the tensile strength, eliminating horizontal cracking in the end zones of the BS12 girder, as shown in Fig. 15. Based on the numerical results, the actual girder was prepared as in case #2, with four debonded strands.

Table 2
Concrete material properties for BS12 girder model.

	Compressive Strength (N/mm^2)	Tensile strength (N/mm^2)	Modulus of elasticity (GPA)	Compressive fracture energy (N/mm)	Tensile fracture energy (N/mm)
Prestressing	35	2.46	29.5	52.1	0.1
Bending test	50	3.12	33	62.93	0.1

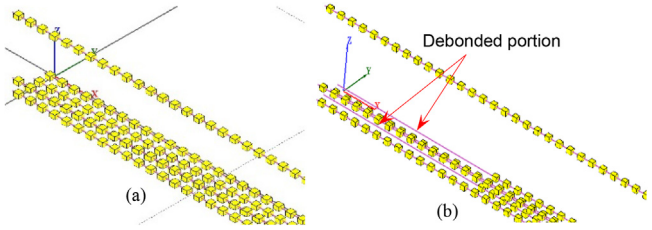

Fig. 8. Prestressing forces in PC strands: (a) Case #1; (b) Case # 2.

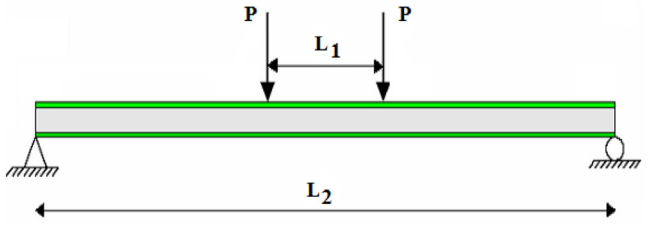

Fig. 10. Application of four–point bending test in the construction stage analysis.

where f_t is the tensile strength, G_t is the tensile fracture energy, G_c is the compressive fracture energy, d_{max} mm is the maximum size of coarse aggregate, and f_c is the concrete compressive strength.

5.2. Construction stage analysis results

The load–displacement and load–strain results obtained from the bending test simulations were analyzed. Fig. 16 shows the displacement of the girder at two locations, at the center and at one–quarter of the girder length. From the displacement and load graphs, it is observed that the girder behaved elastically until the yield point and began to deform with lower stiffness. Fig. 17 shows the compressive and tensile strains at the top and bottom fibers of the girder as a function of the applied load. The overall strain response remained elastic until the yield point before the strains started to increase.

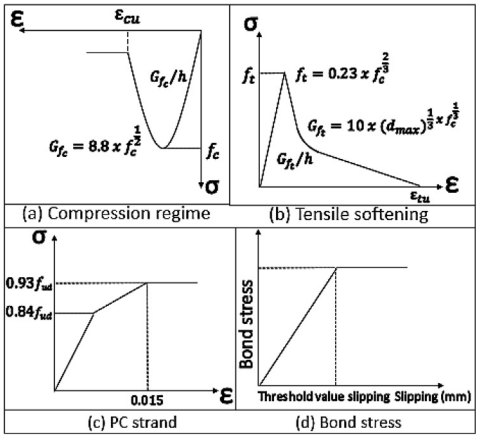

Fig. 11. Constitutive laws for analysis models [29].

6. Experimental program

6.1. Construction procedure

The experiment was conducted on a pretensioned hollow–type BS12 girder to obtain test data to validate the numerical model. The girder was fabricated in a factory with identical characteristics, dimensions, and material properties as those in the numerical model. The girder was 12500 mm long with a 12000 mm span length and a 640 mm × 500 mm effective cross–sectional area. Steel stirrups 10 mm in diameter with different spacings along the girder were provided to resist torsion at the middle and shear forces at the ends of the girder. The girder was prestressed by 12 PC strands 15.2 mm in diameter to provide the required stiffness. The girder consisted of four longitudinal segments divided by three intermediate and two ending diaphragms, and the hollow parts were filled with cork, as shown in Fig. 18.

6.2. Prestressing stage

Once the strands were placed in the cross–section and prepared for pretensioning, pretensioning forces were applied using

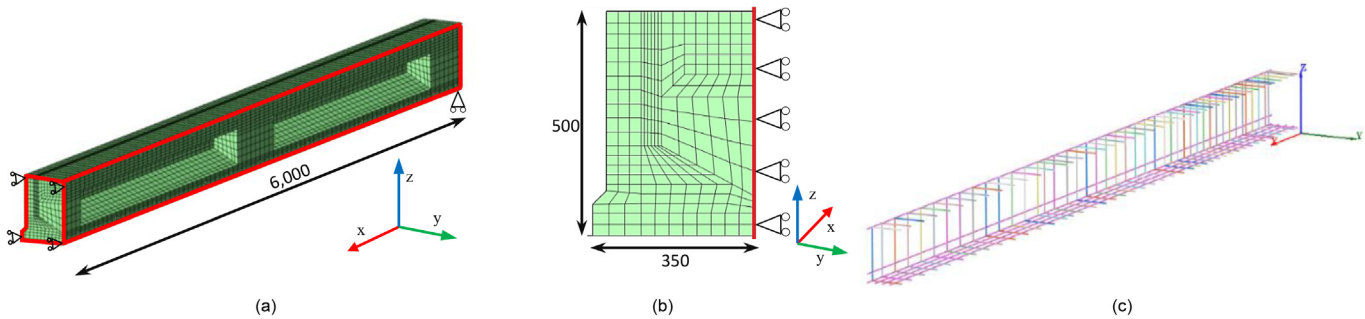

Fig. 9. (a) Longitudinal model (red line denotes one–quarter of the double symmetry), (b) Cross–sectional view, and (c) reinforcement model.

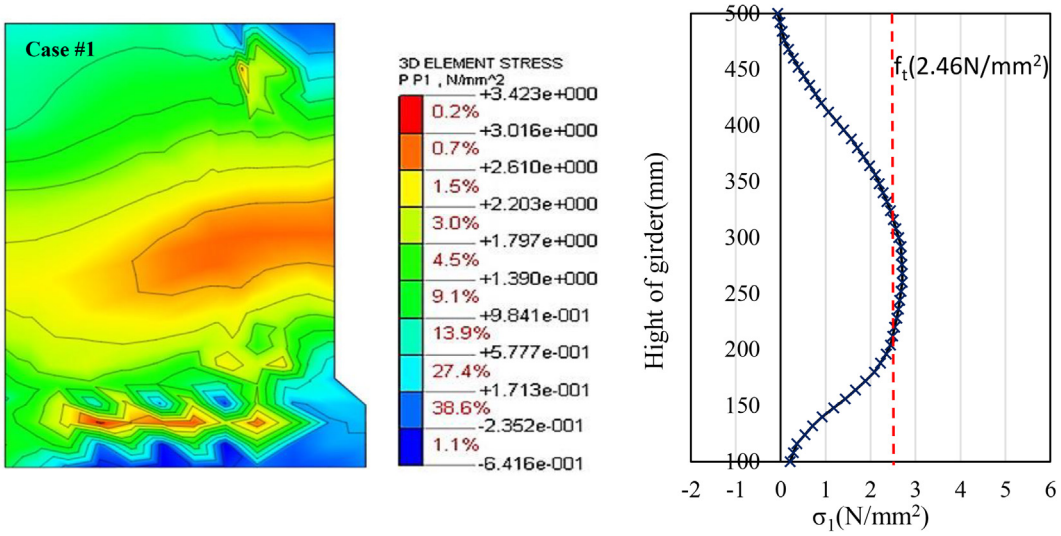

Fig. 12. Principal stresses in the half cross–section of girder in Case #1.

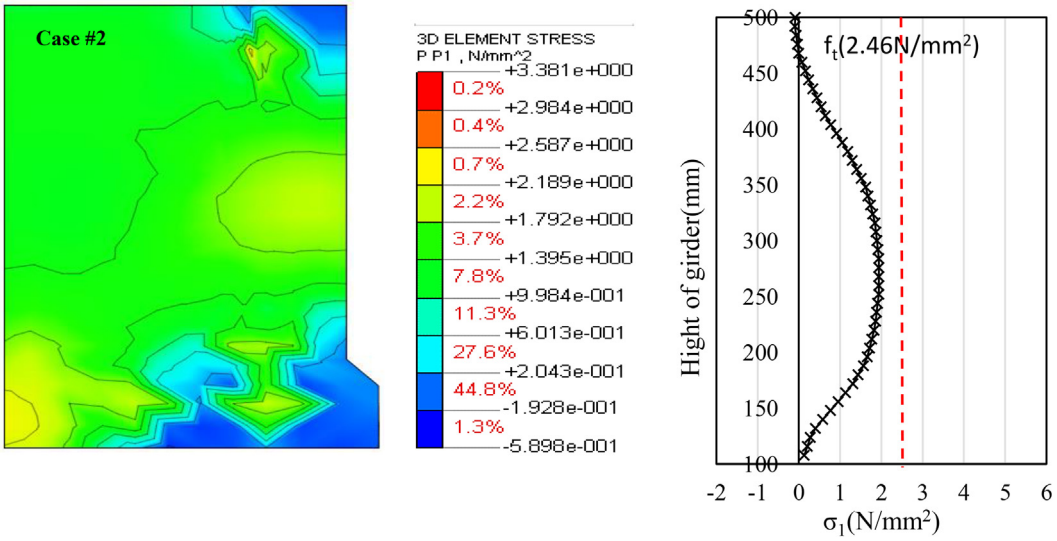

Fig. 13. Principal stresses in the half cross–section of girder in Case #2.

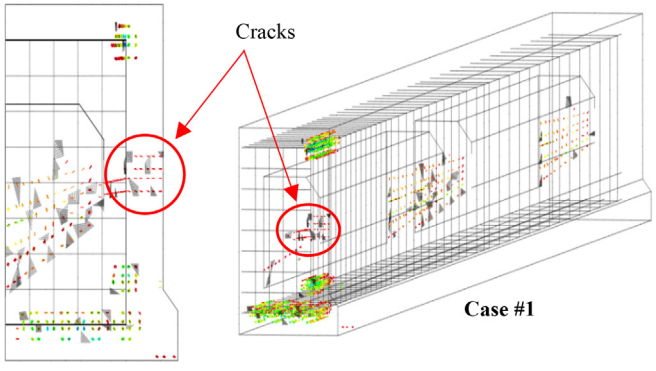

Fig. 14. End zone of girder with horizontal cracks.

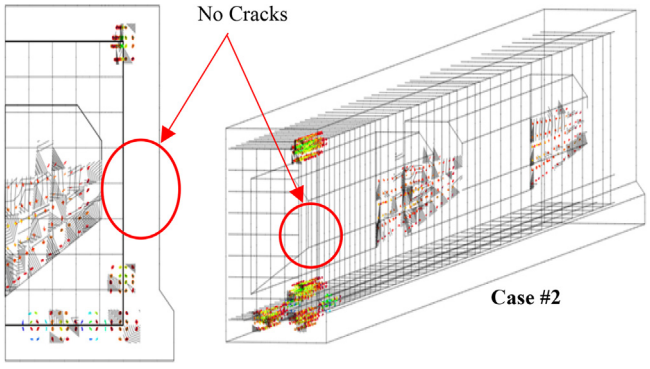

Fig. 15. End zone of girder without horizontal cracks.

hydraulic jacks and gradually increased to a limit load of 187.2 kN on each strand, as shown in Fig. 19. The strand–debonding process was initiated by debonding four alternating strands with an equal transfer length (988 mm) in the tension zone (lower flange) of the girder using a softer debonding material consisting of a polymer plastic closed tube (polyvinyl chloride

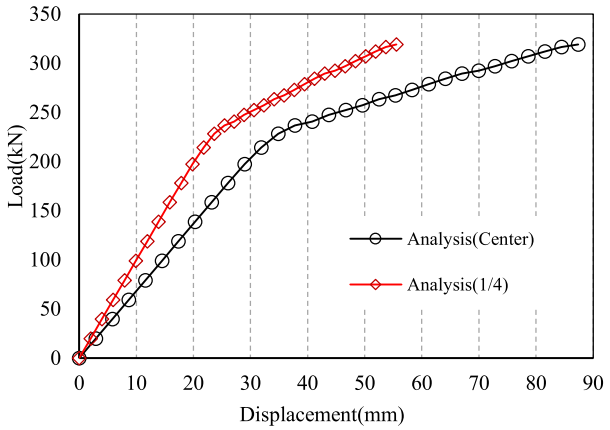

Fig. 16. Load–displacement results of numerical model.

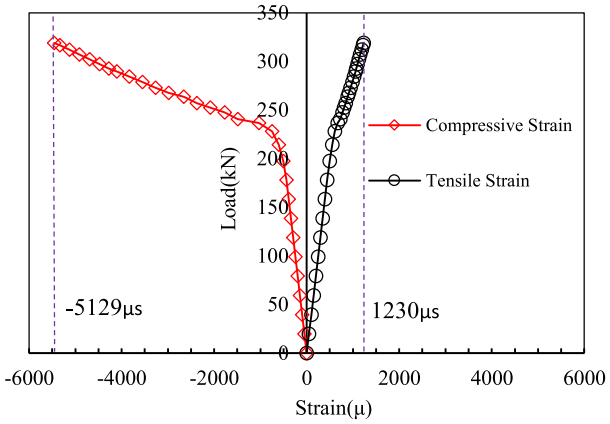

Fig. 17. Numerical model compressive and tensile strains at the middle of top and bottom girder fibers.

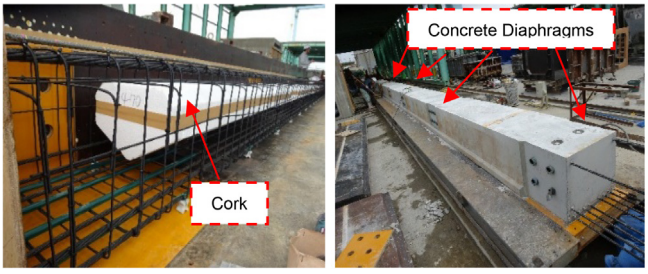

Fig. 18. Specimen overview in experimental field.

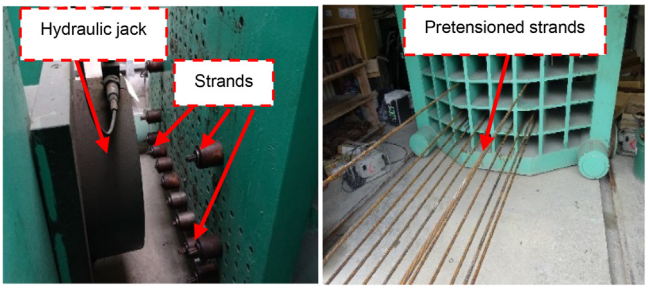

Fig. 19. Prestressing force applied to the strands.

pipe) with a diameter of 20 mm to eliminate bond effects between the strands and the concrete.

The girder was equipped with three 100 mm KM–100–type strain gauges connected to a data acquisition system (DAQ) to obtain the strains at the girder end where the prestress transfer takes place, as shown in Figs. 20 and 21. When concrete reaches its cracking limit and the stress magnitude abruptly decreases, the stress does not accurately describe the condition of the tested member in this case, although the strain still develops and indicates the loading condition. Thus, the strain was measured experimentally to investigate the behavior of the girder under several conditions; strain measurements were preferred over stresses. The corresponding effective stresses were computed from the measured strains using Hooke's law in Eq. (5).

$$\sigma = E \times \varepsilon \tag{5}$$

where σ denotes the stress in the concrete, E is the elastic modulus, and ε is the measured strain.

6.3. Detensioning

Detensioning was initiated by reducing the oil pressure on the hydraulic jack after 70% of the concrete strength was confirmed following 18 h of steam curing, as shown in Fig. 22. The process

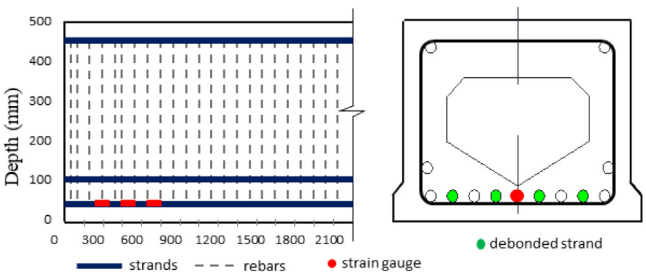

Fig. 20. Position of strands, debonded strands, and strain gauges.

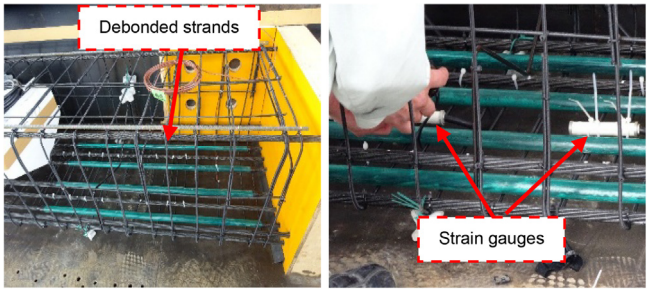

Fig. 21. Debonded strands and strain gauges at end of girder.

Fig. 22. Steam curing and detensioning process.

of gradually reducing the forces on all (fully bonded and debonded) strands was continued until the prestress force was fully transferred from the strands to the concrete. Data was recorded in steps during detensioning, immediately after detensioning, and after the removal of the girder from the experimental bed.

6.4. Bending test

The full strength of the girder was confirmed by testing the concrete cylinders after two weeks of casting. A bending test was conducted to evaluate the load–bearing capacity of the girder, assuming the girder to be a simply supported beam. A static load was applied at two points on the mid–span of the girder using a hydraulic jack, as shown in Fig. 23a. To determine the vertical deflection behavior of the girder, two displacement meters were mounted on the bottom fiber of the girder, one at the center and another at one–quarter of the span length (1/4L), as shown in Fig. 23b. External strain gauges were attached to the upper and lower surfaces at the center of the girder to obtain the strains, as shown in Fig. 24. To identify the tensile and compressive stresses, the strains were converted to stresses using Hooke's law. The load was applied starting from zero and gradually increased to 335 kN. Some small surface cracks appeared in the mid–bottom area during loading but disappeared upon full unloading of the girder, demonstrating the linear–elastic bearing behavior of the girder

7. Experimental results

7.1. Strain readings

Experimental data recording began with the monitoring of the girder end zones where horizontal cracks occurred upon the release of strands after the completion of detensioning. Table 3 lists the measured strains and the corresponding effective stresses obtained from the three strain gauges at the end of the BS12 girder immediately after the strand release process. The strains measured by the embedded gauges are shown in Fig. 25.

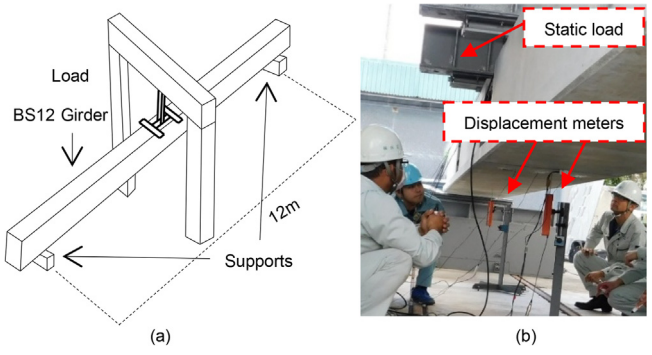

Fig. 23. (a) Bending test schematic; (b) Positions of displacement meters.

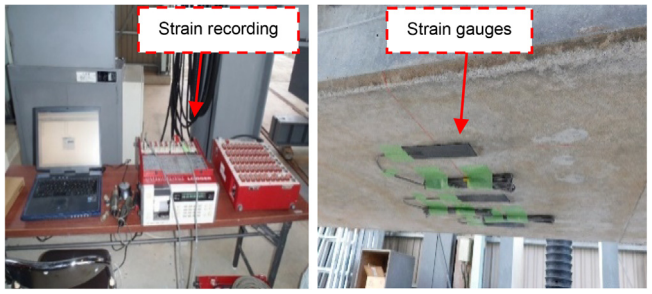

Fig. 24. Position of surface strain gauges and strain measurement.

Table 3
Experimental measured strains and corresponding effective stresses.

Gauge Number	#1	#2	#3
Gauge distance from the end (mm)	300	550	800
Measured strain (μs)	229.72	210.04	249.4
Effective stress (N/mm2)	7.581	6.931	8.230

7.2. Bending test results

The bending test results indicated that the load–bearing capacity and reaction of the BS12 girder were in line with those expected under actual loading. The performance of the girder was consistent in terms of deflection and surface strain, showing a smooth proportional response to an increase in load. The girder reached its full strength in accordance with the design values; cracks started to appear after the load exceeded the design yield strength, as shown in Fig. 26. The cracks continued to increase in length and aperture as the load increased. The girder fractured in the middle of the upper fiber of the compression zone upon reaching an applied load of 335 kN, as shown in Fig. 27. The measurements of the embedded strain gauges on the upper and lower surfaces of the girder indicated tensile and compressive strains during the loading process, as shown in Fig. 28.

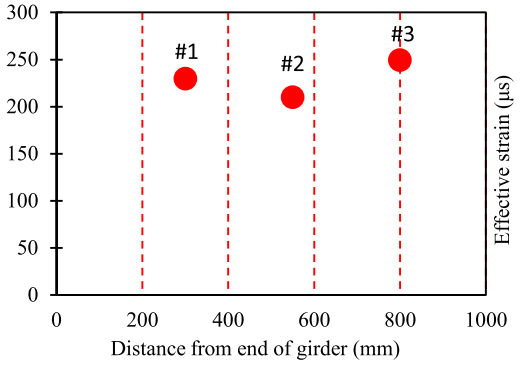

Fig. 25. Experimental strains along girder length after prestressing.

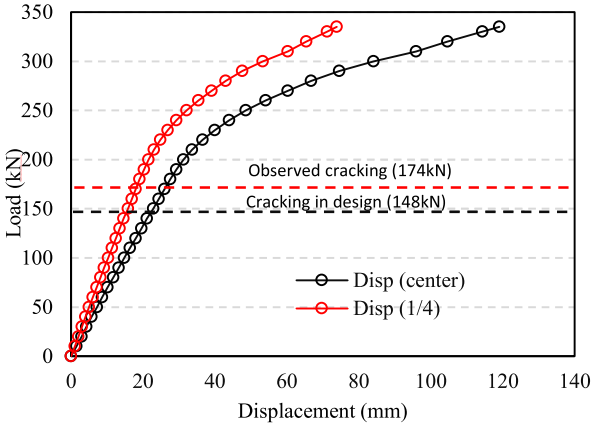

Fig. 26. Load–displacement relationship during bending test.

8. Discussion

Horizontal cracks occur at the ends of pretensioned girders during prestress release because prestress forces are transferred from the strands to the concrete. In this study, a method based on strand–debonding to effectively eliminate horizontal cracks at the ends of a pretensioned hollow–type BS12 girder was examined through a numerical study and verified by experimental results. The parameters considered in this method were the length, configuration, and number of selected debonded strands.

The girder was modeled using MIDAS FEA software to simulate two cases. In the Case #1 model, all strands were fully bonded. In Case #2, four alternating strands were debonded in the bottom row in the tension zone of the girder. In Case #1, the magnitude of the principal stresses at the ends of the girder was observed to be greater than the tensile strength of the concrete. Thus, horizontal cracks occurred at the ends of the girder. However, in Case #2, by debonding four strands over a distance equal to the transfer length at the girder end, the magnitude of the principal stresses decreased to a level less than the tensile strength of the concrete, resulting in no cracking in the end zone of the girder.

To verify the obtained numerical results, the girder was fabricated in a factory using Case #2 for both ends. Both ends of the girder were monitored throughout the procedure, from pretensioning to the end of detensioning. The method successfully reduced the principal stresses below the tensile strength of the concrete by debonding specific strands to eliminate horizontal cracking at the ends of the girder.

The effective stress distribution was assessed at the lowermost concrete fiber for the entire length using FEA, and compared with the effective stresses obtained from the experiment and the theoretical design value. The numerical effective stress values were in good agreement with the experimental values and the theoretical values from Eq. (1), as shown in Fig. 29.

Based on the numerical and experimental results, the principal stresses upon strand release can be controlled and reduced to a level less than the tensile strength of the concrete by debonding strands in specific numbers, positions, and lengths, preventing horizontal cracking at the ends of BS12 and similar girders.

Load–bearing capacity is another concern in hollow–type girders because they have a hole in the cross–section through the entire length; this feature was considered in this study. A numerical model of the girder was created using a construction stage analysis in FEA to investigate the load–bearing capacity of the girder under vertical loading. The measured numerical results in the form of load–strain and load–displacement curves were in accordance with values recorded from the strain gauges and displacement meters attached to the girder during the four–point bending test in the experimental program, and proved the elastic behavior of the girder.

To validate the obtained results, load–strain and load–displacement curves of FEA model and experimental model were compared. Fig. 30 indicates the good agreement of both numerical and experimental results by showing bearing capability of hollow–type girders against vertical loads. Moreover, tensile and compressive strains of FEA model and experiment were also quite reliable as seen in Fig. 31.

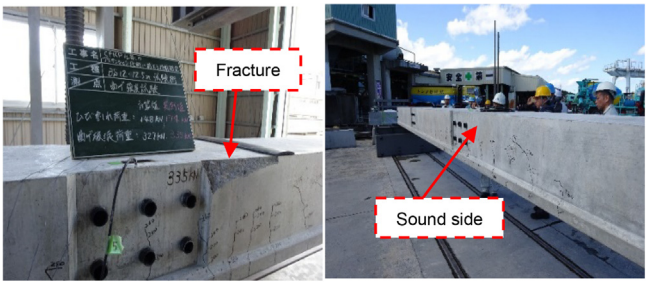

Fig. 27. BS12 girder condition after bending test.

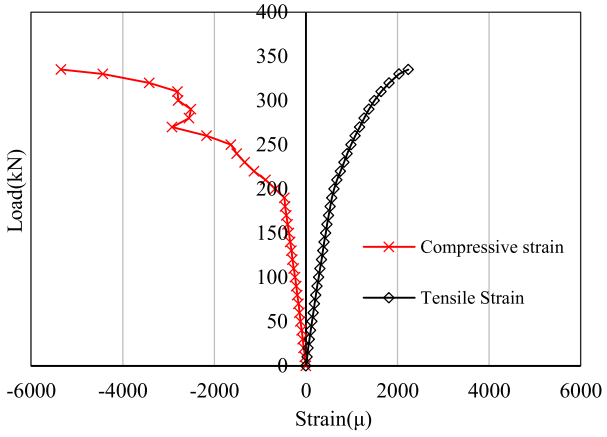

Fig. 28. Load–strain relationship during experimental bending test.

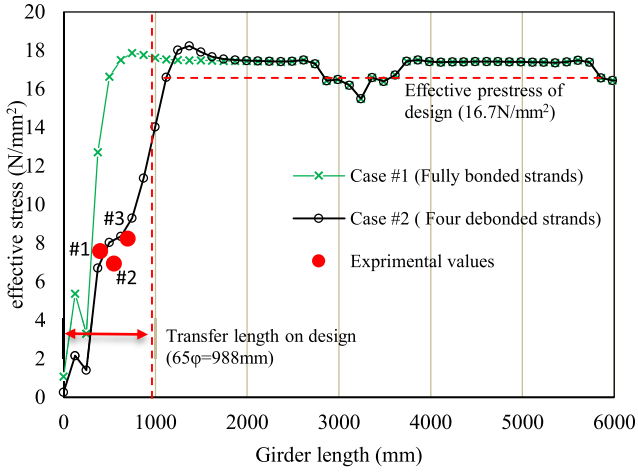

Fig. 29. Comparison of numerical and experimental effective stresses with the design value.

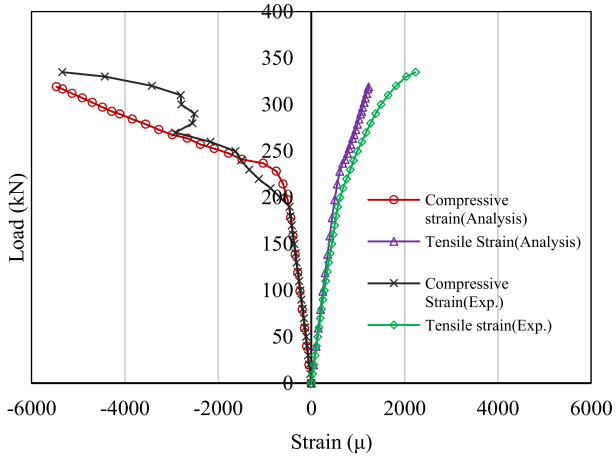

Fig. 30. Comparison of numerical and experimental compressive and tensile strains.

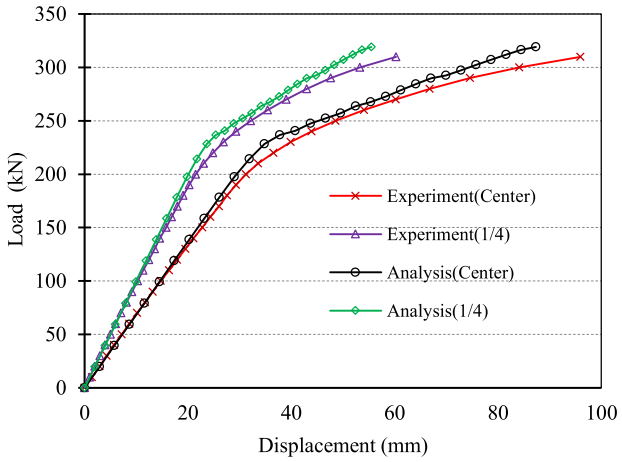

Fig. 31. Comparison of numerical and experimental load–displacement curves.

9. Conclusions

The purpose of this study was to implement a strand–debonding method that can control horizontal cracks at the ends of a pretensioned hollow–type BS12 girder that may occur during and immediately after the strand release process. The load–bearing capacity of such girders was also a primary concern; it was confirmed that the load–bearing capacity of hollow–type pretensioned girders is not a concern. The numerical simulation results were verified experimentally; the conclusions of this study are as follows.

- Experimental and numerical (finite element analysis) results were remarkably similar to each other.
- Debonding four strands in the lower flange of the BS12 girder with a distance equal to the transfer length directly reduced the amplitude of principal stresses below the tensile strength of the concrete upon detensioning. Thus, horizontal cracks did not occur at the ends of the girder.
- The study confirmed that without additional end reinforcements, only the strand–debonding method can prevent horizontal end cracks in the girder.
- Debonding strands with certain specifications was considered for prestressed hollow–type BS12 girders. This method can be adopted for girders with specifications similar to the BS12 girder.
- The construction stage analysis of MIDAS FEA revealed that pretensioned hollow–type girders have sufficient load–bearing capacity, similar to girders with ordinary cross–sections; this was experimentally verified through load–strain and load–displacement curves obtained from the four–point bending test.

Declaration of Competing Interest

The authors declare that they have no known competing financial interests or personal relationships that could have appeared to influence the work reported in this paper.

Acknowledgements

The authors would like to sincerely acknowledge Dr. Ömer Aydan, Emeritus Professor of the University of the Ryukyus for help and advice during this study and in the preparation of this manuscript, as well as the collaboration of Giken Corporation in Okinawa, Japan, for providing the opportunity to prepare the BS12 girder for experimental work.

References

[1] F. Bai, J. Davidson, Composite beam theory for pretensioned concrete structures with solutions to transfer length and immediate prestress losses, Eng. Struct. 126 (2016) 739–758, https://doi.org/10.1016/j.engstruct.2016.08.031.
[2] P. Okumus, M. Oliva, S. Becker, Nonlinear finite element modeling of cracking at ends of pretensioned bridge girders, Eng. Struct. 40 (2012) 267–275, https://doi.org/10.1016/j.engstruct.2012.02.033.
[3] B.A. Aasim, A.K. Karimi, J. Tomiyama, Ö. Aydan, Numerical verification of accelerometer-based assessment of hollow-type pretensioned concrete girder, Asian J. Civ. Eng. 21 (2020) 437–447, https://doi.org/10.1007/s42107-019-00219-w.
[4] P. Okumus, M. Oliva, Evaluation of crack control methods for end zone cracking in prestressed concrete bridge girders, PCI J. 58 (2) (2013) 91–105, https://doi.org/10.15554/pcij.03012013.91.105.
[5] A.B. Sturm, P. Visintin, R. Seracino, G.W. Lucier, D.J. Oehlers, Flexural performance of pretensioned ultra-high performance fibre reinforced concrete beams with CFRP tendons, Compos. Struct. 243 (2020) 112223, https://doi.org/10.1016/j.compstruct.2020.112223.
[6] M. Sanabra Loewe, J. Capellà Llovera, The four ages of early prestressed concrete structures, PCI J. 59 (4) (2014) 93–121.
[7] D.P. Billington, Historical perspective on prestressed concrete, PCI J. 49 (1) (2004).
[8] J. Yang, J. Kim, D. Yoo, Transfer length in full-scale pretensioned concrete beams with 1.4 m and 2.4 m section depths, Eng. Struct. 171 (2018) 433–444, https://doi.org/10.1016/j.engstruct.2018.05.104.
[9] A. Shafiei Dastgerdi, R.J. Peterman, A. Savic, K. Riding, B.T. Beck, Prediction of splitting crack growth in prestressed concrete members using fracture toughness and concrete mix design, Constr. Build. Mater. 246 (2020) 118523, https://doi.org/10.1016/j.conbuildmat.2020.118523.
[10] P.H. Kaar, N.W. Hanson, Bond fatigue tests of beams simulating pretensioned concrete crossties, PCI J. 20 (5') (1975) 65–80.
[11] J. Martí-Vargas, P. Serna, J. Navarro-Gregori, J. Bonet, Effects of concrete composition on transmission length of prestressing strands, Constr. Build. Mater. 27 (1) (2012) 350–356, https://doi.org/10.1016/j.conbuildmat.2011.07.038.
[12] W.L. Gamble, Field Investigation of A Continuous Composite Prestressed I-beam Highway Bridge Located in Jeffeson County, University of Illinois Engineering Experiment Station. College of Engineering. University of Illinois at Urbana-Champaign, Illinois, 1970.
[13] C. Vázquez-Herrero, I. Martínez-Lage, F. Martínez-Abella, Transfer length in pretensioned prestressed concrete structures composed of high performance lightweight and normal-weight concrete, Eng. Struct. 56 (2013) 983–992, https://doi.org/10.1016/j.engstruct.2013.06.020.
[14] H. Svensson, Cable-Stayed Bridges: 40 Years of Experience Worldwide, John Wiley & Sons, 2013.
[15] B.A. Aasim, M.S.G.A. Rahman, A.K. Karimi, J. Tomiyama, Y. Yoshitsugu, & A. Higa. Vibration-based comparison of accelerometer and microtremor sensors with numerical verification by assessing a PC-bridge.
[16] A. Nasiri, T. Shimozato, Y. Mumtaz. Experimental study on the post-cracking behavior of preflex beams under cyclic loading. In Structures (Vol. 29, pp. 1390-1403). Elsevier. DOI:10.1016/j.istruc.2020.12.023.
[17] R. Burgueño, & Y. Sun. Effects of debonded strands on the production and performance of prestressed concrete beams (No. RC-1546) (2011).
[18] P. Okumus, & M.G. Oliva. Strand debonding for pretensioned bridge girders to control end cracks. ACI Structural Journal, 201. (2014), 111(1). DOI:10.14359/51686518.
[19] A. Abdelatif, J. Owen, M. Hussein, Modelling the prestress transfer in pretensioned concrete elements, Finite Elem. Anal. Des. 94 (2015) 47–63, https://doi.org/10.1016/j.finel.2014.09.007.
[20] A.K. Karimi, B.A. Aasim, J. Tomiyama, Y. Suda, Ö. Aydan, K. Kaneda, Experimental and numerical studies on the control of horizontal cracking at the ends of hollow-type pretensioned girders, SN Appl. Sci. 2 (10) (2020) 1–17, https://doi.org/10.1007/s42452-020-03461-z.
[21] B. Atmaca, Ş. Ateş, M. Günaydin, A.C. Altunişik, Effects of strand configuration on pre-tensioned I-girders, Sigma J. Eng. Natural Sci./Mühendislik ve Fen Bilimleri Dergisi 36 (1) (2018).
[22] Japanese Industrial Standards (JIS A 5373 - 2010).
[23] J. Benítez, J. Gálvez, Bond modelling of prestressed concrete during the prestressing force release, Mater. Struct. 44 (1) (2010) 263–278, https://doi.org/10.1617/s11527-010-9625-5.
[24] Japanese Industrial Standards (JIS G 3536 – 2014).
[25] Japan Society of Civil Engineers (2007). Standard Specifications for Concrete Structures, Tokyo, Japan.
[26] Japan Road Association (2012). Specification of Highway Bridges, part 3, Concrete Bridges. Maruzen, Japan.
[27] F. Leonhardt, Prestressed concrete: Design and construction, W. Ernst, 1964.
[28] M. Osman, & C. French. Debonded Strands in Prestressed Concrete Bridge Girders (2019).
[29] Finite Element Analysis algorithm, MIDAS FEA.